J. Fluid Mech. (2024), *vol*. 997, A29, doi:10.1017/jfm.2024.841

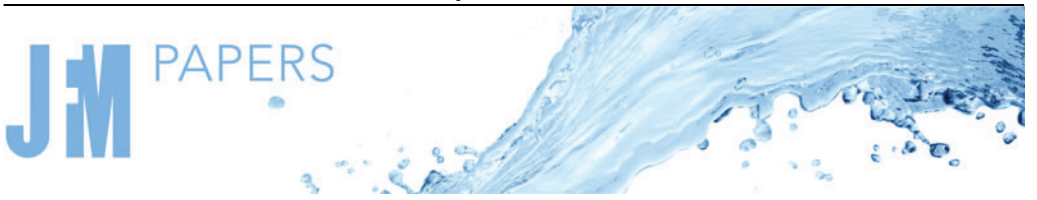

Phase segregation of a partially miscible binary mixture subjected to an external force field

Chih-Che Chueh[1],†, **Roberto Mauri**[2] **and Antonio Bertei**[2],†

[1]Department of Aeronautics and Astronautics, National Cheng Kung University, Tainan 701, Taiwan

[2]Department of Civil and Industrial Engineering, University of Pisa, Largo Lucio Lazzarino 2, 56122 Pisa, Italy

(Received 28 March 2024; revised 1 August 2024; accepted 2 September 2024)

When a partially miscible binary mixture is quenched below its critical temperature, it transitions from its single-phase to a two-phase region, undergoing phase separation. The processes of formation and coalescence of droplets are driven by diffusive and convective phenomena, taking place isotropically in the system. The application of an external force field, which exerts a different contribution on the two species, breaks the symmetry of phase separation, leading to the segregation of two equilibrated phases separated by a single interface. This study investigates the dynamics of phase segregation under an external force. The effects of various force magnitudes, captured by the Bond number, in both high- and low-viscosity mixtures, distinguished by different fluidity numbers, are quantified via numerical simulations by using the phase field model. The intricate dynamics of formation, floating and coalescence of droplets towards complete segregation are described along with the quantification of the segregation time, revealing different patterns for high and low Bond numbers. Results show that in none of the cases, formation and floating can be regarded as strictly serial processes. A universal scaling between segregation time, Bond number, fluidity number and domain size is not possible, with a power-law dependence emerging only under the diffusion-dominated regime.

Key words: suspensions, breakup/coalescence, Marangoni convection

1. Introduction

The temperature-composition phase diagram of a partially miscible liquid mixture at a given pressure exhibits two distinct regions: a stable sector where the mixture is homogeneous, indicating complete miscibility of the liquids, and a two-phase region where two homogeneous phases coexist. These regions are separated by the equilibrium

† Email addresses for correspondence: chuehcc@mail.ncku.edu.tw, antonio.bertei@unipi.it

curve, obtained through the minimization of the mixture's free energy. When a partially miscible binary mixture is brought from the single-phase to the two-phase region by altering its composition and/or temperature, a phase separation process occurs. This process involves the formation of droplets of the minority phase, which subsequently grow by diffusion and coalescence. Close to the equilibrium curve within the two-phase region of the phase diagram, the mixture exists in a metastable state, necessitating a finite activation energy to initiate the phase separation process. Conversely, far from the equilibrium curve, the mixture becomes unstable, leading to phase separation via spinodal decomposition (Gunton, San Miguel & Sahni 1983; Gunton 1984; Binder 2005). This process entails the growth of fluctuations, even infinitesimal ones, exceeding a critical wavelength.

The growth of droplets of the minority phase in the context of phase separation is due to the relative movement of the two phases, induced by diffusion and convection. Diffusion arises from molecular velocity fluctuations at equilibrium, wherein molecules undergo incoherent, random motion without any specific preferential direction. In contrast, convection is a collective phenomenon that occurs over larger distances and is influenced by both outer and inner force fields. The latter is described by the diffuse interface model (also known as the phase field model) (Hohenberg & Halperin 1977; Anderson, McFadden & Wheeler 1998; Lowengrub & Truskinovsky 1998; Lamorgese, Mauri & Sagis 2017; Bertei, Chueh & Mauri 2021) as the gradient of a non-equilibrium chemical potential. Under equilibrium conditions, this, so-called, Korteweg force reduces to the Marangoni force (Jasnow & Viñals 1996; Jacqmin 2000), allowing the phase field approach to be viewed as a generalized model based on surface tension (McGuire *et al.* 1996; Martula *et al.* 2000), whereby the force acting on droplets linearly increases with their interface area. In the absence of an outer force field, both diffusion and convection occur in random directions, resulting in the formation of isotropic morphological structures. The ratio between convection and diffusion magnitudes is captured by the fluidity number, which distinguishes low viscous mixtures from high viscous ones. Notably, when diffusion dominates, as in the case of highly viscous systems or shallow temperature quenches, the average radius of the drops grows over time following a $t^{1/3}$ (Siggia 1979; deGennes 1980; Lifshitz & Pitaevskii 1984) or more generalized power law (Binder & Stauffer 1974; Binder 1977; Midya & Das 2017). Conversely, when convection drives the process, as seen in low-viscosity liquid mixtures or deep temperature quenches, the mean droplet radius grows linearly with time (Siggia 1979; Tanaka 1996), in agreement with numerous experimental results (Chou & Goldburg 1979; Wong & Knobler 1981; Guenoun *et al.* 1987; Cumming *et al.* 1992; White & Wiltzius 1995; Gupta, Mauri & Shinnar 1999; Mauri *et al.* 2003; Califano & Mauri 2004).

The force exerted on droplets by an outer force field exhibits a linear growth with respect to the droplet volume, in contrast to the force resulting from the inner force field, which depends on the droplet surface area. The ratio between these two forces is referred to as the Bond number, which exhibits a linear dependence on the droplet radius. Consequently, for small droplets characterized by small Bond numbers, the outer force can be disregarded, resulting in isotropic morphological structures. As the droplets grow, they eventually reach a critical size corresponding to an $O(1)$ Bond number, known as the capillary length. At this point, the influence of the outer force field becomes significant, causing a breakdown in the process symmetry. Recent research has demonstrated that when the mixture is initially unstable, phase separation occurs rapidly through spinodal decomposition, leading to a complete segregation of the two phases. In contrast, for initially metastable mixtures, the external force primarily induces species stratification, followed by a much slower nucleation process (Bertei & Mauri 2022).

This study focuses on examining the phase separation process and its progression towards complete segregation. Numerical simulations are performed for different Bond and fluidity numbers, thus investigating the dynamics of segregation for both diffusion-dominated and convection-dominated regimes at different extents of the external force field. After presenting the model equations in § 2, numerical results are first discussed qualitatively in § 3.1, highlighting the principal phenomena of formation, coalescence and progression towards thermodynamic equilibrium with and without an external force field. A quantitative analysis of segregation, formation and floating times is then presented in § 3.2, revealing that phase segregation cannot be strictly interpreted as a series of elementary phenomena, although some patterns for the segregation time as a function of Bond number emerge in the diffusion-dominated regime.

2. Physical and mathematical model descriptions

The dynamic behaviour of a regular binary mixture under the influence of an external force field has been studied in previous works (Bertei & Mauri 2022; Chueh, Mauri & Bertei 2022) for Mauri's non-equilibrium multiphase flow group. The physical model is developed based on the principles of mass conservation, momentum conservation and conservation of chemical species. The model assumes isothermal conditions and makes the following assumptions: (i) constant density, viscosity and diffusion coefficient that are independent of composition; and (ii) a regular and symmetric mixture, whose excess enthalpy depends on the Margules parameter Ψ (Bertei *et al.* 2021), where the two species possess equal molecular weights. This assumption is not overly restrictive and serves as a simplification to reduce the number of parameters. It is worth noting that for polymeric mixtures with high molecular weight, the average molecular weight can be used. As a result, the governing equations can be simplified as follows:

$$\nabla \cdot \boldsymbol{v} = 0, \tag{2.1}$$

$$\rho\left(\frac{\partial \boldsymbol{v}}{\partial t} + \boldsymbol{v}\cdot\nabla\boldsymbol{v}\right) + \nabla p = \eta\nabla^2\boldsymbol{v} + \rho\boldsymbol{f}, \tag{2.2}$$

$$\rho\left(\frac{\partial \phi}{\partial t} + \boldsymbol{v}\cdot\nabla\phi\right) + \nabla\cdot\boldsymbol{J}_\phi = 0, \tag{2.3}$$

where ρ is the density of the mixture and η is its viscosity, while $\boldsymbol{v}$, p and ϕ are respectively the mass-averaged velocity, the pressure and the mass fraction of species 1, which are functions of position, $\boldsymbol{r}$, and time, t. Furthermore, $\boldsymbol{f}$ and $\boldsymbol{J}_\phi$ are the force per unit mass and the diffusive flux of species 1, respectively. In the present study, $\boldsymbol{f}$ is the sum of the outer (gravitational or electric) force, $\boldsymbol{f}^{(ext)}$, and the inner Korteweg non-equilibrium force, $\boldsymbol{f}^{(K)}$ (Bertei & Mauri 2022):

$$\rho\boldsymbol{f} = \rho\left(\boldsymbol{f}^{(K)} + \boldsymbol{f}^{(ext)}\right) = -\rho\phi\nabla(\psi_{12}^{(K)} + \psi_{12}^{(ext)}) = -\rho\phi\nabla\psi_{12}^{(cons)}, \tag{2.4}$$

where $\psi_{12}^{(K)} = -R'Ta^2\nabla^2\phi$ is the Korteweg potential difference and $\psi_{12}^{(ext)} = -\chi_{12}bz$ is the external potential difference. Here, $R' = R/M_w$ (with R denoting the universal gas constant and M_w the molecular weight), T is the temperature (that here is assumed to be uniform), a is a characteristic length (which is proportional to the surface tension at equilibrium), $b = |\boldsymbol{b}|$ is the external force field magnitude, acting along the z-direction, and χ_{12} is the susceptibility difference, indicating how differently the two components of the mixture respond to the applied field. Note that a total energy potential

$\psi_{12}^{(cons)} = \psi_{12}^{(K)} + \psi_{12}^{(ext)}$ can be defined as the sum of all the conservative body forces (namely, Korteweg and external forces).

According to non-equilibrium thermodynamics, the diffusive flux, $\boldsymbol{J}_\phi$, can be written as (Bertei & Mauri 2022)

$$\boldsymbol{J}_\phi = -D^* \boldsymbol{\nabla} \left(\mu_{12} + \psi_{12}^{(cons)} \right), \tag{2.5}$$

where μ_{12} is the thermodynamic chemical potential (which can be derived from the free energy of the mixture), while D^* is the effective diffusivity. Imposing that for ideal mixtures (2.5) must reduce to Fick's law, then we obtain $D^* = (\rho D/R'T)\phi(1-\phi)$, where D is a constant diffusivity.

It is important to mention that the energy balance equation has been omitted in this analysis. This decision is based on the assumption that, similar to liquids, heat propagates significantly faster than mass. Consequently, it is assumed that the temperature of the mixture remains constant and uniform, mimicking an instantaneous quench.

After substituting the expressions for the non-equilibrium Korteweg force, the external force and the diffusion flux into the governing equations (2.1)–(2.3), we can transform them into a dimensionless form using the following scaling:

$$\tilde{\boldsymbol{x}} = \frac{\boldsymbol{x}}{\hat{a}}, \quad \tilde{t} = \frac{t}{\hat{a}^2/D}, \quad \tilde{\boldsymbol{v}} = \frac{\boldsymbol{v}}{D/\hat{a}}, \quad \tilde{p} = \frac{p}{\eta D/\hat{a}^2}. \tag{2.6a–d}$$

Here, $\hat{a}$ stands for the characteristic length, $\hat{a}^2/D$ denotes a characteristic diffusion time, $D/\hat{a}$ is a characteristic diffusion velocity, while $\eta D/\hat{a}^2$ represents a scaling factor for pressure. Consequently, the governing equations that describe the conservation of mass, momentum and chemical species are as follows:

$$\tilde{\boldsymbol{\nabla}} \cdot \tilde{\boldsymbol{v}} = 0, \tag{2.7}$$

$$N_{Sc}^{-1} \left(\frac{\partial \tilde{\boldsymbol{v}}}{\partial \tilde{t}} + \tilde{\boldsymbol{v}} \cdot \tilde{\boldsymbol{\nabla}} \tilde{\boldsymbol{v}} \right) + \tilde{\boldsymbol{\nabla}} \tilde{p} = \tilde{\nabla}^2 \tilde{\boldsymbol{v}} + N_\alpha \phi \tilde{\boldsymbol{\nabla}} (\tilde{\nabla}^2 \phi + N_{Bo} \tilde{z}), \tag{2.8}$$

$$\frac{\partial \phi}{\partial \tilde{t}} + \tilde{\boldsymbol{\nabla}} \cdot (\tilde{\boldsymbol{v}} \phi + \tilde{\boldsymbol{J}}_\phi) = 0;$$

$$\tilde{\boldsymbol{J}}_\phi = -\left[(1 - 2\Psi\phi(1-\phi)) \tilde{\nabla}\phi - \frac{\Psi}{2} \phi(1-\phi) \tilde{\nabla} (\tilde{\nabla}^2 \phi + N_{Bo} \tilde{z}) \right], \tag{2.9}$$

where the following dimensionless parameters are defined: the Schmidt number, the fluidity number and the Bond (or Eotvos) number:

$$N_{Sc} = \frac{\eta}{\rho D}, \quad N_\alpha = \frac{\rho R' T_c \hat{a}^2}{\eta D}, \quad N_{Bo} = \frac{\chi_{12} b \hat{a}}{R' T_c}. \tag{2.10a–c}$$

The Schmidt number, N_{Sc}, represents the ratio of momentum diffusivity (η/ρ) to material diffusivity (D). Note that in (2.6), N_{Sc} assumes a role similar to that of the inverse Reynolds number, so that for liquid mixtures, where $N_{Sc} \gg 1$, the inertial term in (2.8) is negligible. In this work, as we consider liquid mixtures, we assume $N_{Sc} = 10^3$. The fluidity number, referred to as N_α, can be interpreted as an intrinsic Péclet number. It provides insight into whether the process is predominantly governed by mass diffusion ($N_\alpha \leq 1$) or by convection ($N_\alpha \gg 1$). Lastly, the Bond (or Eotvos) number, denoted as N_{Bo}, expresses the ratio between external and capillary forces. The representative external force is given by $\rho \chi_{12} b \hat{a}^3$, while the reference capillary force is $\hat{\sigma}\hat{a}$, where $\hat{\sigma}$ represents a reference surface

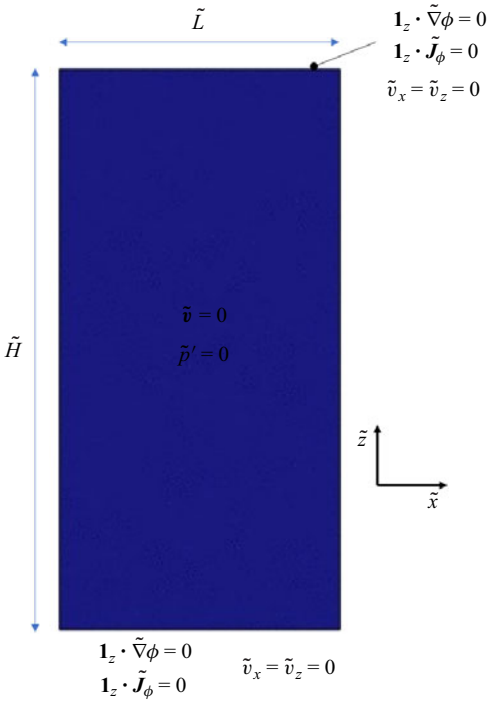

Figure 1. Initial and boundary conditions considered in the present study.

tension equal to $\hat{\sigma} = \rho R' T_c \hat{a}$ (Chueh *et al.* 2022), where T_c is the critical temperature of the mixture. Both forces are expressed relative to the intrinsic characteristic length, $\hat{a}$. The Bond number can also be viewed as the ratio between the characteristic interface length $\hat{a}$ and the capillary length, $l_c = R' T_c / \chi_{12} b$.

The system of (2.7)–(2.9) is solved numerically in a two-dimensional domain $\Omega = (\tilde{x}, \tilde{z})$, which represents a rectangular region with lateral periodic boundaries with two dimensionless side lengths of $\tilde{H}$ and $\tilde{L}$, as depicted in figure 1. The initial conditions of the mixture are characterized by a state of rest, indicated by $\tilde{\boldsymbol{v}} = 0$, and uniform pressure, represented by $\tilde{p} = 0$.

An initial mass fraction lying within the spinodal unstable region (Sandler 2006) is set to $\phi_0 = 0.4$, accompanied by a superimposed random white noise ε with statistical properties $\langle \delta\phi \rangle = 0$ and $\langle \delta\phi^2 \rangle^{1/2} = 10^{-2}$ at $t = 0$. These conditions indicate an abrupt and uniform quenching of the mixture below its critical temperature, with a Margules parameter Ψ set equal to 2.62.

3. Results and discussion

In § 3.1, we explore the detailed complexities related to representing phase transition patterns, specifically focusing on the changes in N_{Bo} and N_α at a given $N_{Sc} = 10^3$. Here, N_α is the ratio between convection- and diffusion-driven material fluxes, and therefore the process is convection driven when $N_\alpha \gg 1$, while it is diffusion driven when $N_\alpha < 1$. In fact, in the absence of external forces, it has been shown (Vladimirova, Malagoli & Mauri 1999) that the mean droplet size, d, grows linearly with time, i.e. $d \propto t$ when $N_\alpha \gg 1$, while $d \propto t^{1/3}$ when $N_\alpha < 1$, in agreement with experimental results (Gupta *et al.* 1999; Mauri

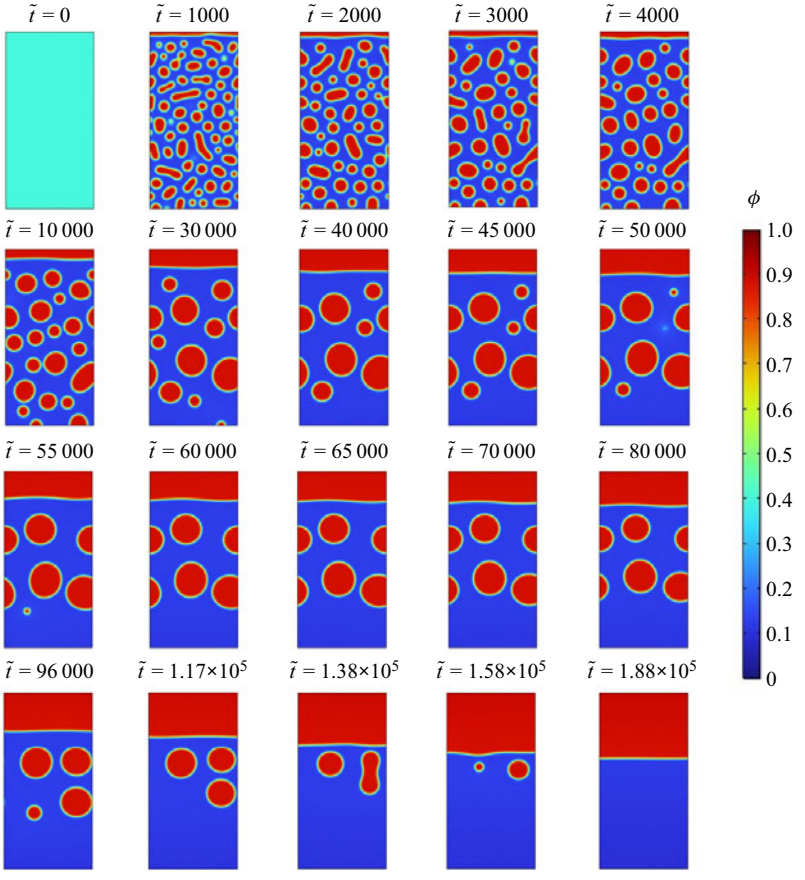

Figure 2. Time evolution of phase segregation for $N_\alpha = 0.01$ and $N_{Bo} = 10^{-3}$ in a rectangular domain with two dimensionless side lengths of $\tilde{H} = 200$ and $\tilde{L} = 100$.

et al. 2003). Conversely, N_{Bo} plays a crucial role in determining the strength of an external force field, which is powerful enough to cause upward movement of the droplets along the z-axis. In § 3.2, correlations for phase separation and phase segregation as functions of domain height, N_{Bo} and N_α, are presented. It is important to note that simulations were carried out using the same code already validated by Chueh, Bertei & Mauri (2020) and Bertei & Mauri (2022).

3.1. *Effect of N_{Bo} and N_α on phase segregation*

Figure 2 illustrates a scenario where both N_α and N_{Bo} are notably small, namely $N_\alpha = 0.01$ and $N_{Bo} = 10^{-3}$. Given the asymmetric initial composition $\phi_0 = 0.4$, phase separation proceeds via the formation of droplets of the minority phase. We see that drops form and start growing due to the coalescence induced by diffusion; However, the convection induced by external forces is initially very weak, since the drops are much smaller than the capillary length l_c, where external forces are balanced by surface forces (i.e. the corresponding macroscopic Bond number is $O(1)$). In the last part of the process, as the drops increase in size, the effect of the external force starts to become relevant, thus facilitating droplet growth through convection-induced coalescence. Note that, despite the

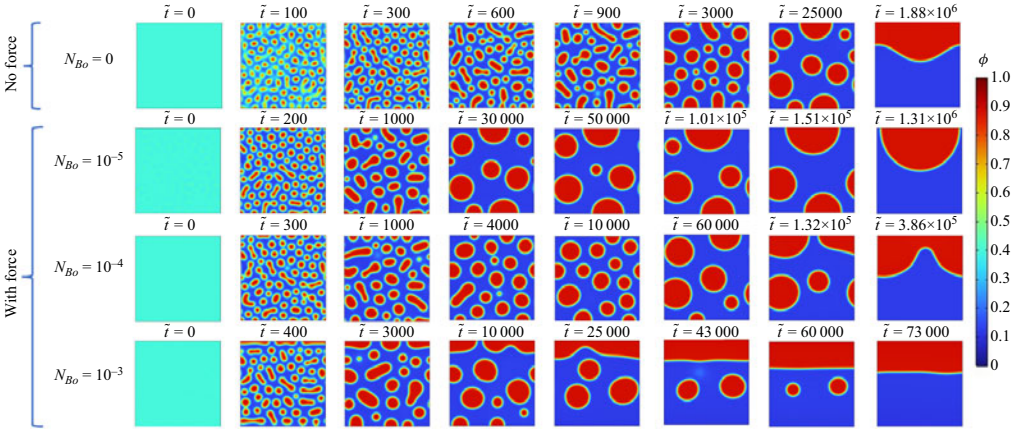

Figure 3. Time evolution of phase segregation for $N_\alpha = 0.01$ and N_{Bo}, ranging from 0 to 10^{-3}, in a square domain with the dimensionless side length of $\tilde{H} = \tilde{L} = 100$.

seemingly small value of N_{Bo}, the external force always plays a significant role, since at the end, drops will always reach the capillary length size and start moving upward; while in the absence of external forces, this floating process does not take place. At the end, we observe the formation of an upper rich phase (in red) with a horizontal interface that moves downward, until complete phase segregation is reached. It is interesting to note that, due to a 90° contact angle, some droplets occasionally remain attached to both the bottom and the upper walls. However, the magnitude of the Bond number, $N_{Bo} = 10^{-3}$, exceeds a critical threshold identified in previous works (Chueh *et al.* 2022), corresponding to the point at which droplets detach from the confining walls. Furthermore, the observed behaviour and dynamics align notably well with the patterns depicted in figure 4 of Califano, Mauri & Shinnar (2005), further corroborating the agreement between the experimental findings and the current study.

It is particularly intriguing to conduct a comparative analysis of the phase separation patterns in the presence and absence of an external force field, as visually demonstrated in figure 3. In the absence of any external force (as depicted in the first row of figure 3), the growth of the droplets is primarily influenced by the effect of the internal force field, which is typically proportional to the area of the interface. As we observe the impact of increasing values of N_{Bo}, ranging from 10^{-5} to 10^{-3}, we see that the external force field, whose effect is proportional to the volume of the drops and grows linearly with their size, becomes increasingly influential. Consequently, the acceleration in the drop formation process becomes more pronounced (notice the different dimensionless times above each panel), thereby expediting the attainment of complete segregation within the system.

A noteworthy transformation is shown in figure 4, as the value of N_α is set to 100, ushering in a distinct dominance of convection within the process at hand. As time progresses, the droplets exhibit a tendency to either emerge or coalesce with one another due to the vigorous influence of convection in a nearly ballistic motion. Consequently, the phenomenon of diffusion-induced growth, observed in previous instances, becomes irrelevant under such circumstances. In a parallel development, when $N_{Bo} < 10^{-4}$, the red drops remain attached to the bottom wall through the capillary force, and the external force is not strong enough to detach them. However, for larger N_{Bo}, the rich red phase embarks on an upward trajectory, progressively forming an interface that moves in a downward

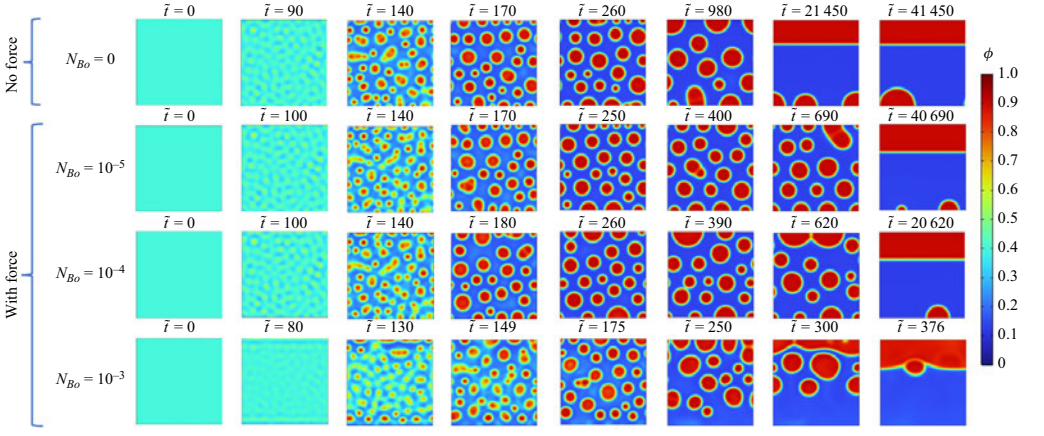

Figure 4. Time evolution of phase segregation for $N_\alpha = 100$ and N_{Bo}, ranging from 0 to 10^{-3}, in a square domain with the dimensionless side length of $\tilde{H} = \tilde{L} = 100$.

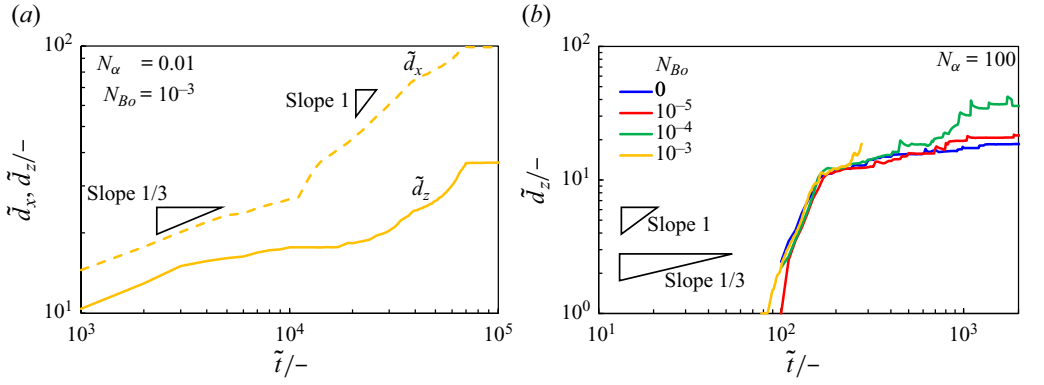

Figure 5. Characteristic droplet size as a function of dimensionless time for (*a*) $N_\alpha = 0.01$ and (*b*) $N_\alpha = 100$ for a selection of Bond numbers corresponding to figures 3 and 4.

direction over time. Overall, the dynamics of the process becomes much faster than in the absence of convection (compare the dimensionless times above each panel in figures 3 and 4).

A comparative analysis of the droplet size evolution is shown in figure 5. The figure reports the characteristic droplet size (Bertei, Tellini & Mauri 2019; Chueh, Bertei & Mauri 2020) along the horizontal ($\tilde{d}_x$) and vertical direction ($\tilde{d}_z$) as a function of dimensionless time for a selection of different Bond numbers in the two regimes of fluidity numbers, corresponding to the cases represented in figures 3 and 4. Figure 5(*a*), corresponding to $N_\alpha = 0.01$ and $N_{Bo} = 10^{-3}$, shows that droplets grow according to a scaling $\tilde{d} \propto \tilde{t}^{1/3}$ as long as they are sufficiently small to be unaffected by the external force field; then, as the droplet size increases, the external force adds a coherent vertical motion that causes coalescence in both directions and speeds up the droplet growth. Nevertheless, the convection-dominated regime, characterized by $\tilde{d} \propto \tilde{t}$, is not reached; this is consistent with the qualitative description provided at the beginning of this section. For $N_\alpha = 100$, reported in figure 5(*b*), in addition to the irregular spikes that correspond to coalescence events, there is a faster growth along the vertical direction as the Bond number increases. The growth rate never scales as $\tilde{d} \propto \tilde{t}^{1/3}$ as expected, because the dynamics is dominated

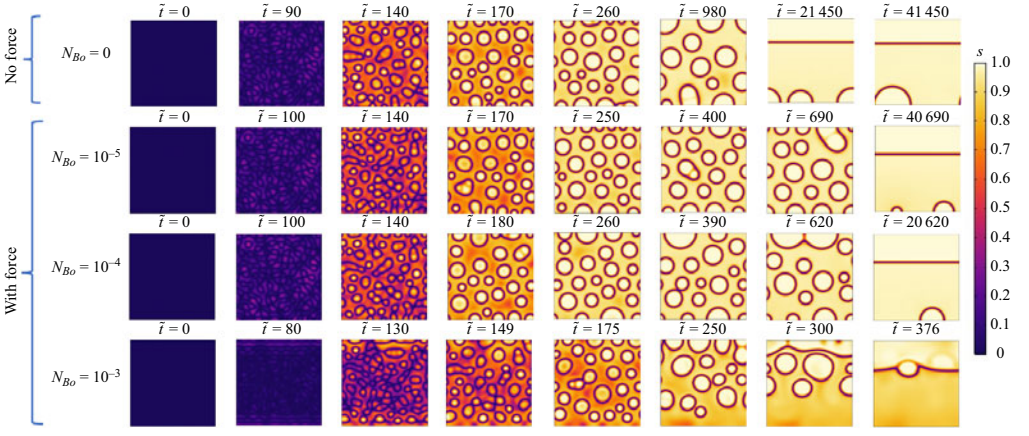

Figure 6. Time evolution of separation depth contour corresponding to figure 4.

by convection for $N_\alpha = 100$, but a clear and sustained linear regime cannot be claimed either as N_{Bo} varies. As also stressed in the next section, identifying general laws for the convection-driven regime is challenging and requires larger computational domains and statistical analysis which are beyond the scope of the present study.

Coming back to the qualitative description of phenomena, it is important to acknowledge that a mixture may initially attain a state of local equilibrium, wherein the compositions of the droplets and the continuous phase align with the equilibrium compositions of the respective phases. However, the complete segregation of the two phases occurs much later in the process. Consequently, we introduce the concept of separation depth to measure the extent to which the system deviates from local equilibrium on a 0–1 scale. The separation depth, S, was defined by Vladimirova, Malagoli & Mauri (1999) as

$$S = \begin{cases} \dfrac{\phi - \phi_0}{\phi_e^{(B)} - \phi_0} & \text{for } \phi > \phi_0 \\ \dfrac{\phi - \phi_0}{\phi_e^{(A)} - \phi_0} & \text{for } \phi \le \phi_0 \end{cases}, \tag{3.1}$$

where $\phi_e^{(A)}$ and $\phi_e^{(B)}$ denote the equilibrium compositions of the poor (blue) and rich (red) phases, equal to 0.12 and 0.88, respectively, for the conditions simulated in this study. For $N_\alpha = 100$, the separation depth maps shown in figure 6 provide a vivid portrayal of the droplets quickly achieving local equilibrium, while the encompassing continuum phase situated outside lingers in a state of disequilibrium. The diffuse interface separating the two phases inherently shows $S < 1$ since the mass fraction varies smoothly from inside to outside a droplet according to the phase field approach. The discrepancy between internal droplet equilibration versus external disequilibrium of the continuum phase, along with the interfacial composition gradient (Kumaran 1998, 2000), serve as crucial factors for the rapid dynamics observed within the system. Although barely noticeable, the external force induces a little variation in composition along the vertical direction in both the continuum and droplet phases, which corresponds to the stratification phenomenon discussed elsewhere (Bertei & Mauri 2022). In any case, it is clear that in a convection-dominated regime, droplets equilibrate quickly after emergence and initial growth, while further coalescence induced by the external force field takes place at a later stage when the droplets are locally at thermodynamic equilibrium.

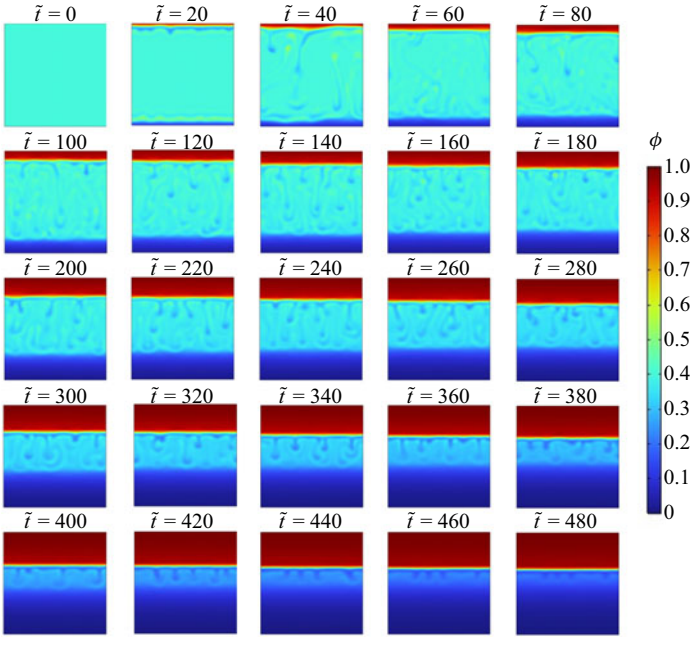

Figure 7. Time evolution of phase segregation for $N_\alpha = 100$ and $N_{Bo} = 10^{-1}$, in a square domain with the dimensionless side length of $\tilde{H} = \tilde{L} = 100$.

In figure 7, when $N_{Bo} = 10^{-1}$ and $N_\alpha = 100$, the strong convection induced by the external force field causes a stratification of the two species, with the formation of two interfaces. Therefore, during the process of phase separation, $\phi \approx \phi_e^{(B)}$ at the top and $\phi \approx \phi_e^{(A)}$ at the bottom, while between the two interfaces, a random convective motion takes place (with no local equilibrium), with a rapid process of spinodal decomposition. Then, the two interfaces gradually move towards each other until they merge and a complete phase segregation is reached. The phase separation process described in figure 7 corresponds to the experimental data by Califano & Mauri (2018).

3.2. *Quantitative analysis of segregation time*

In this section, we present a quantitative analysis of the processes that were qualitatively described in the previous section. In particular, so far, we loosely defined segregation as the process that leads to a complete separation of the two equilibrated phases, A and B, under an external force. Being more specific, we mark the segregation time, $\tilde{t}_{segr}$, as the time at which there is, within the domain, only one interface that separates the two equilibrated phases. Thus, $\tilde{t}_{segr}$ characterizes the segregation process at the macroscale, by identifying the moment when the system transitions from multiple interfaces to a single interface. Arguably, the segregation process may be decoupled into two phenomena: (i) formation, which is the process of emergence of droplets until their internal composition achieves thermodynamic equilibrium; and (ii) floating, which refers to the rising and coalescence of (equilibrated) droplets under the external force field (obviously, we would call this process sedimentation if droplets moved downwards, which depends only on the orientation of the external force field). Each of these two processes takes place in a finite time that we call $\tilde{t}_{form}$ and $\tilde{t}_{floa}$ for formation and floating, respectively.

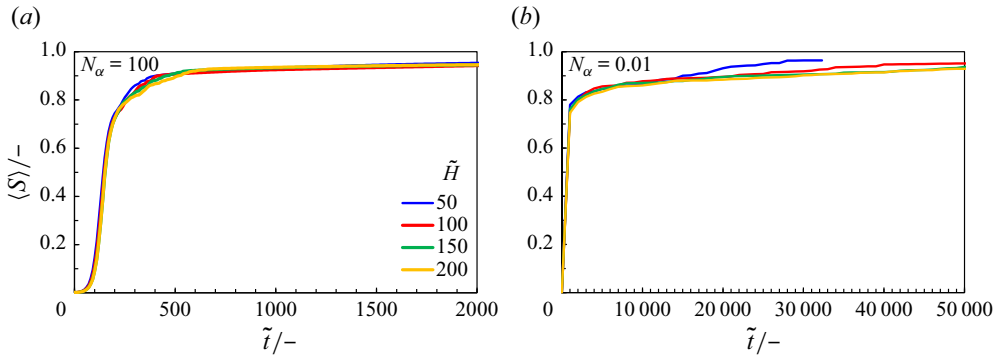

Figure 8. Change in average separation depth over dimensionless time for different dimensionless domain heights for (*a*) $N_\alpha = 100$, (*b*) $N_\alpha = 0.01$, given $N_{Bo} = 10^{-3}$.

For large Bond numbers, we cannot refer to independent formation and floating as distinct processes, as shown in figure 7 for $N_{Bo} = 10^{-1}$, where no droplets form and two well-separated regions grow from the top and the bottom at the expense of the central mixed region. For smaller Bond numbers, instead, we may speculate that formation and floating take place in series. In fact, while phase separation initially occurs on a small scale and does not depend on the presence of an external force, corresponding to the formation stage, the rise and progressive coalescence of droplets is mainly dictated by the external force field during the floating stage, eventually leading to complete segregation of the phases. We may also speculate that formation, being a process occurring locally and dictated by how far the system is from equilibrium, is independent of the domain dimension, namely the domain height $\tilde{H}$, so that any dependence of the segregation time from the domain size has to be attributed to the floating time. Thus, it seems reasonable to assume that the segregation time can be obtained as the sum of the formation time and floating time, that is,

$$\tilde{t}_{segr}(\tilde{H}) = \tilde{t}_{form} + \tilde{t}_{floa}(\tilde{H}), \tag{3.2}$$

with the brackets denoting the dependence of a term from the domain height. This ansatz is critically investigated in this section by addressing first the formation time and then the floating time.

Since the formation refers to the emergence of droplets and their thermodynamic equilibration, it seems natural to use the separation depth, S, as a useful metric to mark the formation time. According to its definition in (3.1), the separation depth is a scalar quantity that measures the deviation from equilibrium locally in each point of the domain. To obtain a global descriptor of the formation within the domain, we adopt the integral average of the separation depth, $\langle S \rangle = (1/\tilde{H}\tilde{L}) \int_\Omega S \, \mathrm{d}\tilde{x} \, \mathrm{d}\tilde{z}$. Figure 8 reports the average separation depth as a function of dimensionless time for different domain heights for two representative fluidity numbers at $N_{Bo} = 10^{-3}$. The average separation depth increases with time in every case indicating that the system evolves towards equilibrium, albeit more slowly for $N_\alpha = 0.01$ since system evolution is ruled by diffusion. Notably, $\langle S \rangle$ never becomes equal to one in a finite system because, even though $S = 1$ within the bulk of the phases, the diffuse interface separating the two phases is characterized by a gradient of composition ϕ and, as such, by $S < 1$ (see figure 6). Nonetheless, $\langle S \rangle$ approaches an asymptotic maximum value at the end of the segregation. Figure 8 also shows that $\langle S \rangle$ is basically independent of the domain height $\tilde{H}$ since, for each value of N_α, all the curves tend to collapse one onto the others. This indicates that $\langle S \rangle$ contains information about the

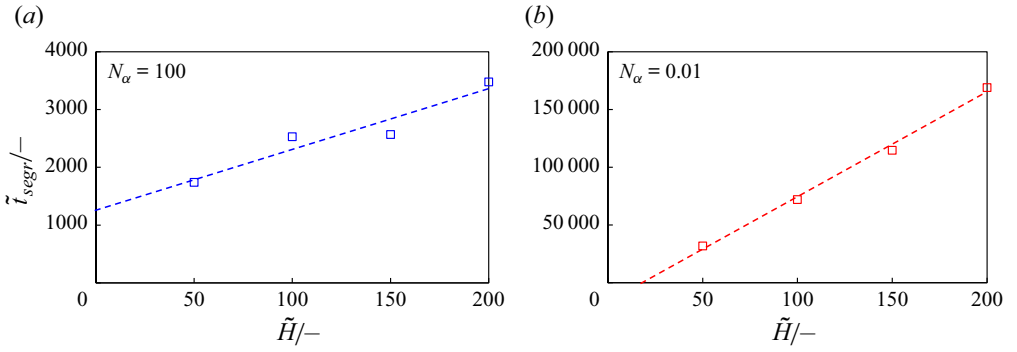

Figure 9. Segregation time as a function of dimensionless domain heights for (*a*) $N_\alpha = 100$, (*b*) $N_\alpha = 0.01$, given $N_{Bo} = 10^{-3}$. The dashed lines denote the best linear fit of data according to the least square method.

system pathway towards equilibrium without being affected by the domain size, which is exactly what the formation process and the formation time aim to mark, satisfying part of the ansatz in (3.2). As such, $\langle S \rangle$ is adopted to identify the formation time $\tilde{t}_{form}$.

Despite setting a threshold value of $\langle S \rangle$ contains a certain degree of arbitrariness, an analysis of figure 6 at $N_\alpha = 100$ reveals that droplets are internally equilibrated (i.e. $S = 1$) at $\tilde{t} \approx 260$, which corresponds to $\langle S \rangle = 0.8$ in figure 8(*a*). Thus, we identify the formation time $\tilde{t}_{form}$ as the time at which $\langle S \rangle$ equals 0.8, which is $\tilde{t}_{form} \approx 260$ for $N_\alpha = 100$. Clearly, at the formation time, $\langle S \rangle$ has not yet approached its asymptotic maximum value because the continuum blue phase is not equilibrated yet at $\phi_e^{(A)} = 0.12$, as denoted by the colourmap in the last row of figure 6 at $N_{Bo} = 10^{-3}$. By using the same threshold $\langle S \rangle = 0.8$ in figure 8(*b*), we find $\tilde{t}_{form} \approx 2000$ for $N_\alpha = 0.01$, independent of the domain height, which consistently agrees with the internal equilibration of the droplets in figure 3 for $N_{Bo} = 10^{-3}$ by judging their colour which is qualitatively similar to that of the droplets at $\tilde{t} \approx 260$ in figure 3 at $N_\alpha = 100$. Therefore, marking $\tilde{t}_{form}$, as the time at which $\langle S \rangle = 0.8$, appears to be a sensible choice to identify the formation process for any value of N_α investigated, while satisfying the requirement of $\tilde{t}_{form}$ being independent of $\tilde{H}$.

Given these premises, the analysis shifts to the identification of the floating time and its additivity to the formation time to give the segregation time, which is a means to test the validity of (3.2). For the same set of simulations discussed in figure 8, figure 9 reports the segregation time $\tilde{t}_{segr}$ as a function of the dimensionless domain height $\tilde{H}$ for $N_\alpha = 100$ and $N_\alpha = 0.01$ at $N_{Bo} = 10^{-3}$. If formation and floating really take place in series according to (3.2), with $\tilde{t}_{form}$ being independent of the domain height as shown above (see figure 8), any dependence of the segregation time with $\tilde{H}$ will scale directly to the floating time $\tilde{t}_{floa}$, with $\tilde{t}_{form}$ representing an offset of $\tilde{t}_{segr}$ versus $\tilde{H}$. The results in figure 9 indicate that, for both high and low fluidity numbers, which denote convection-driven and diffusion-driven phase separation and segregation, the segregation time increases with the domain height following a fairly linear trend, indicated by the dashed lines. However, in figure 9(*a*), the offset, which should correspond to $\tilde{t}_{form}$, is equal to 1200, which is much larger than $\tilde{t}_{form} \approx 260$ identified above at $N_\alpha = 100$ from the analysis of the separation depth at the threshold $\langle S \rangle = 0.8$. By looking at the last row in figure 4, it is clear that at $\tilde{t} = 1200$, the formation is completed and the floating has already started. However, figure 9(*b*) indicates that the extrapolation of the linear trend gives a negative offset for $N_\alpha = 0.01$, which would mean a negative $\tilde{t}_{form}$, which has no physical meaning.

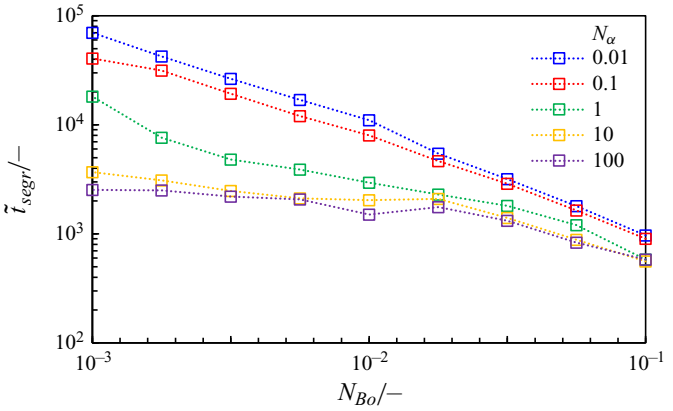

Figure 10. Segregation time as a function of Bond number for different values of N_α, given the dimensionless height $\tilde{H} = 100$.

Hence, both these observations indicate that formation and floating are not strictly processes occurring in series and the latter may not scale strictly linearly with the domain height, which is the scaling one would expect in case the external force would pull the droplets at a constant terminal velocity. More importantly, the analysis of data in figure 9 disproves (3.2), meaning that the segregation time cannot be decoupled as a simple sum of formation and floating times, neither for large Bond numbers for which (3.2) is obviously inapplicable (see figure 7) nor for relatively small Bond numbers (namely, $N_{Bo} = 10^{-3}$ as shown here). We conclude that formation and floating take place partly in series and partly in parallel in a convoluted manner. This result is independent from the few arbitrary choices made above, such as marking $\tilde{t}_{form}$ at $\langle S \rangle = 0.8$, as any other threshold value would not make (3.2) to hold.

Having assessed that, in general, the segregation time cannot be decoupled as a sum of formation and floating times, figure 10 illustrates the relationship between $\tilde{t}_{segr}$ and Bond number for various values of N_α at a given domain height. Numerical results show that $\tilde{t}_{segr}$ decreases as the Bond number and fluidity number increase, due to the larger pull of the external force field promoting floating in the first case and the higher mobility of droplets in a convective regime in the second case. Nonetheless, universal quantitative trends do not clearly emerge from figure 10. For $N_\alpha \leq 0.1$, a linear dependence with a slope of *ca*. 0.9 in the log-log plot appears, so that the segregation time follows a power scaling with Bond number as $\tilde{t}_{segr} \approx N_{Bo}^{-0.9}$, being independent of N_α the more N_{Bo} approaches 10^{-1}. However, for $N_\alpha \geq 1$, such a power-law scaling does not hold anymore, probably due to an increased influence of convection. In fact, as discussed in § 3.1, the dynamics of phase segregation in the presence of an external force becomes very rich and complex in the convection-dominated regime, with arguably synergic nonlinear phenomena that contribute to phase segregation. The reproducibility and consistency observed across different simulations provide confidence in the validity (or absence thereof) of the scaling, emphasizing the importance of considering the interplay between convection, diffusion, external force and other factors on phase segregation dynamics.

4. Conclusions

The phase field approach was applied in this work to conduct numerical simulations of phase segregation in a partially miscible binary mixture subjected to an external force

field. The presence of an external force breaks the symmetry of phase separation: although the formation of droplets is rather unaffected by the force field, the following coalescence process is no longer isotropic under an external force, which causes the segregation of equilibrated phases separated by a single interface. The dynamics of phase segregation is orders of magnitude slower for fluidity numbers smaller than one (i.e. in diffusion regime), while system evolution becomes much faster and richer in morphological patterns when convection dominates for fluidity number of the order of 100. In all the cases, an increase in Bond number reduces the segregation time. For small Bond numbers (e.g. $N_{Bo} = 10^{-3}$), it is shown that the formation process is independent of the domain height for all the fluidity numbers. Nonetheless, the segregation time increases with the domain height. In any case, formation and floating cannot be regarded as strictly serial processes, so that the segregation time cannot be decoupled as a simple sum of a formation and a floating time. This is also corroborated in the extreme condition of high Bond numbers ($N_{Bo} = 10^{-1}$), when droplet formation does not occur and phase segregation takes place via stratification of equilibrated phases at the boundaries of the domain with two interfaces that move one towards the other while the central mixed region shrinks. A universal scaling between segregation time, Bond number and fluidity number is not possible, although a power-law dependence $\tilde{t}_{segr} \approx N_{Bo}^{-0.9}$ is attained for $N_\alpha \leq 0.1$.

The study and its results promote a deeper and mechanistic understanding of phase segregation, fostering relevant applications where an external force field is imposed to expedite the phase separation process. Future studies will be dedicated to investigating the effects of oscillating force fields on phase separation dynamics.

Supplemental movie. Supplementary movie is available at https://doi.org/10.1017/jfm.2024.841.

Funding. This research received partial funding from the Headquarters of University Advancement at the National Cheng Kung University, which was sponsored by the Ministry of Education, Taiwan, and the National Science and Technology Council (NSTC), Taiwan, under grant No. 111-2221-E-006-102-MY3.

Declaration of interests. The authors report no conflict of interest.

Nomenclature.

a	characteristic length of the diffuse interface [m]
b	external field magnitude [N kg^{-1}]
d_x	characteristic droplet size along direction x [m]
d_z	characteristic droplet size along direction z [m]
D	composition-independent diffusivity [m^2 s^{-1}]
$\boldsymbol{f}$	conservative force per unit mass [N kg^{-1}]
H	domain height [m]
L	domain length [m]
l_c	capillary length [m]
$\boldsymbol{J}_\phi$	diffusive mass flux of species 1 [kg (m^2 s)$^{-1}$]
N_{Bo}	Bond (or Eotvos) number [−]
N_{Sc}	Schmidt number [−]
N_α	fluidity number [−]
p	pressure [Pa]
R'	ideal gas constant per unit mass [J (kg K)$^{-1}$]
S	separation depth [−]
t	time [s]
T	absolute temperature [K]
T_c	critical temperature of the mixture [K]
$\boldsymbol{v}$	mass-average fluid velocity [m s^{-1}]
x	x coordinate [m]
$\boldsymbol{x}$	vector of spatial coordinate [m]
z	z coordinate [m]

Greek letters

ε	random white noise [−]
η	mixture dynamic viscosity [kg (m s)$^{-1}$]
μ_{12}	chemical potential difference [J kg^{-1}]
ρ	mixture density [kg m^{-3}]
ϕ	mass fraction of species 1 [−]
χ_{12}	susceptibility difference [−]
Ψ	Margules coefficient [−]
ψ_{12}	potential energy difference [J kg^{-1}]
Ω	computational domain [−]

Superscripts

$\wedge$	characteristic value of temperature and composition-dependent quantities
$\sim$	physical quantity recast in dimensionless form
A	continuum (remainder) phase
B	droplet phase
cons	conservative
ext	external
K	Korteweg

Subscripts

e	equilibrium
i	species *i*
floa	floating
form	formation
segr	segregation
0	initial

Author ORCIDs.
Chih-Che Chueh https://orcid.org/0000-0001-7065-6900;
Roberto Mauri https://orcid.org/0000-0001-9594-0035;
Antonio Bertei https://orcid.org/0000-0002-3202-6825.

References

Anderson, D.M., McFadden, G.B. & Wheeler, A.A. 1998 Diffuse-interface methods in fluid mechanics. *Annu. Rev. Fluid Mech.* **30**, 139–165.

Bertei, A., Chueh, C.-C. & Mauri, R. 2021 Dynamics of phase separation of sheared binary mixtures after a nonisothermal quenching. *Phys. Rev. Fluids* **6**, 094302.

Bertei, A. & Mauri, R. 2022 Phase separation of a binary mixture with an external force field. *Chem. Engng Sci.* **263**, 118128.

Bertei, A., Tellini, B. & Mauri, R. 2019 Dynamic transition of dendrite orientation in the diffusive spinodal decomposition of binary mixtures under a thermal gradient. *Chem. Engng Sci.* **203**, 450–463.

Binder, K. 1977 Theory for the dynamics of "clusters." II. Critical diffusion in binary systems and the kinetics of phase separation. *Phys. Rev.* B **15**, 4425–4447.

Binder, K. 2005 *Spinodal Decomposition, in Systems Far from Equilibrium*, pp. 76–90. Springer.

Binder, K. & Stauffer, D. 1974 Theory for the slowing down of the relaxation and spinodal decomposition of binary mixtures. *Phys. Rev. Lett.* **33**, 1006–1009.

Califano, F. & Mauri, R. 2004 Drop size evolution during the phase separation of liquid mixtures. *Ind. Engng Chem. Res.* **43**, 349–353.

Califano, F. & Mauri, R. 2018 Retardation of the phase segregation of liquid mixtures with a critical point of miscibility. *AIChE J.* **64**, 4047–4052.

Califano, F., Mauri, R. & Shinnar, R. 2005 Large-scale, unidirectional convection during phase separation of a density-matched liquid mixture. *Phys. Fluids* **17**, 94109.

Chou, Y.C. & Goldburg, W.I. 1979 Phase separation and coalescence in critically quenched isobutyric-acid—water and 2,6-Lutidine—water mixtures. *Phys. Rev.* A **20**, 2105–2113.

CHUEH, C.-C., BERTEI, A. & MAURI, R. 2020 Dynamics of phase separation of sheared inertialess binary mixtures. *Phys. Fluids* **32**, 023307.

CHUEH, C.-C., MAURI, R. & BERTEI, A. 2022 The detachment of a wall-bound pendant drop suspended in a sheared fluid and subjected to an external force field. *Phys. Fluids* **34**, 073306.

CUMMING, A., WILTZIUS, P., BATES, F.S. & ROSEDALE, J.H. 1992 Light-scattering experiments on phase-separation dynamics in binary fluid mixtures. *Phys. Rev.* A **45**, 885–897.

DEGENNES, P.G. 1980 Dynamics of fluctuations and spinodal decomposition in polymer blends. *J. Chem. Phys.* **72**, 4756–4763.

GUENOUN, P., GASTAUD, R., PERROT, F. & BEYSENS, D. 1987 Spinodal decomposition patterns in an isodensity critical binary fluid: direct-visualization and light-scattering analyses. *Phys. Rev.* A **36**, 4876–4890.

GUNTON, J.D. 1984 The dynamics of random interfaces in phase transitions. *J. Stat. Phys.* **34**, 1019–1037.

GUNTON, J.D., SAN MIGUEL, M. & SAHNI, P.S. 1983 The dynamics of first order phase transitions. In *Phase Transition and Critical Phenomena* (ed. C. Domb & J.L. Lebowitz), vol. 8. Academic Press.

GUPTA, R., MAURI, R. & SHINNAR, R. 1999 Phase separation of liquid mixtures in the presence of surfactants. *Ind. Engng Chem. Res.* **38**, 2418–2424.

HOHENBERG, P.C. & HALPERIN, B.I. 1977 Theory of dynamic critical phenomena. *Rev. Mod. Phys.* **49**, 435–479.

JACQMIN, D. 2000 Contact-line dynamics of a diffuse fluid interface. *J. Fluid Mech.* **402**, 57–88.

JASNOW, D. & VIÑALS, J. 1996 Coarse-grained description of thermo-capillary flow. *Phys. Fluids* **8**, 660–669.

KUMARAN, V. 1998 Droplet interaction in the spinodal decomposition of a fluid. *J. Chem. Phys.* **109**, 7644–7648.

KUMARAN, V. 2000 Spontaneous motion of droplets during the demixing transition in binary fluids. *J. Chem. Phys.* **112**, 10984–10991.

LAMORGESE, A., MAURI, R. & SAGIS, L.M.C. 2017 Modeling soft interface dominated systems: a comparison of phase field and gibbs dividing surface models. *Phys. Rep.* **675**, 1–54.

LIFSHITZ, E.M. & PITAEVSKII, L.P. 1984 *Physical Kinetics*. Pergamon Press.

LOWENGRUB, J. & TRUSKINOVSKY, L. 1998 Quasi–incompressible Cahn–Hilliard fluids and topological transitions. *Proc. R. Soc. Lond.* A *Math. Phys. Engng Sci.* **454**, 2617–2654.

MARTULA, D.S., HASEGAWA, T., LLOYD, D.R. & BONNECAZE, R.T. 2000 Coalescence-induced coalescence of inviscid droplets in a viscous fluid. *J. Colloid Interface Sci.* **232**, 241–253.

MAURI, R., CALIFANO, F., CALVI, E., GUPTA, R. & SHINNAR, R. 2003 Convection-driven phase segregation of deeply quenched liquid mixtures. *J. Chem. Phys.* **118**, 8841–8846.

MCGUIRE, K.S., LAXMINARAYAN, A., MARTULA, D.S. & LLOYD, D.R. 1996 Kinetics of droplet growth in liquid–liquid phase separation of polymer–diluent systems: model development. *J. Colloid Interface Sci.* **182**, 46–58.

MIDYA, J. & DAS, S.K. 2017 Kinetics of vapor-solid phase transitions: structure, growth, and mechanism. *Phys. Rev. Lett.* **118**, 165701.

SANDLER, S.I. 2006 *Chemical, Biochemical and Engineering Thermodynamics*, IV ed. Wiley.

SIGGIA, E.D. 1979 Late stages of spinodal decomposition in binary mixtures. *Phys. Rev.* A **20**, 595–605.

TANAKA, H. 1996 Coarsening mechanisms of droplet spinodal decomposition in binary fluid mixtures. *J. Chem. Phys.* **105**, 10099–10114.

VLADIMIROVA, N., MALAGOLI, A. & MAURI, R. 1999 Two-dimensional model of phase segregation in liquid binary mixtures. *Phys. Rev.* E **60**, 6968–6977.

WHITE, W.R. & WILTZIUS, P. 1995 Real space measurement of structure in phase separating binary fluid mixtures. *Phys. Rev. Lett.* **75**, 3012–3015.

WONG, N.-C. & KNOBLER, C.M. 1981 Light-scattering studies of phase separation in isobutyric acid + water mixtures: hydrodynamic effects. *Phys. Rev.* A **24**, 3205–3211.